Biomaterials Advances 155 (2023) 213674

Contents lists available at ScienceDirect

Biomaterials Advances

journal homepage: www.journals.elsevier.com/materials-science-and-engineering-c

Development of accessible platforms to promote myofibroblast differentiation by playing on hydrogel scaffold composition

Alice Cappitti [a,1], Francesco Palmieri [b,1], Rachele Garella [b], Alessia Tani [c], Flaminia Chellini [c], Martina Salzano De Luna [d], Camilla Parmeggiani [a,e], Roberta Squecco [b,*], Daniele Martella [a,e,f,**], Chiara Sassoli [c]

[a] Department of Chemistry "Ugo Schiff", University of Florence, 50019 Sesto Fiorentino, Italy
[b] Department of Experimental and Clinical Medicine, Section of Physiological Sciences, University of Florence, 50134 Florence, Italy
[c] Department of Experimental and Clinical Medicine, Section of Anatomy and Histology, Imaging Platform, University of Florence, 50134 Florence, Italy
[d] Department of chemical, materials and industrial production engineering, University of Naples Federico II, 80125 Napoli, Italy
[e] European Laboratory for Non-Linear Spectroscopy (LENS), 50019 Sesto Fiorentino, Italy
[f] Istituto Nazionale di Ricerca Metrologica (INRiM), 10135 Torino, Italy

ARTICLE INFO

Keywords:
Mechanomimetic materials
Hydrogels
Myofibroblast differentiation
Polyacrylamide
Fibrosis

ABSTRACT

Mechanomimetic materials are particularly attractive for modeling *in vitro* fibroblast to myofibroblast (Myof) transition, a key process in the physiological repair of damaged tissue, and recognized as the core cellular mechanism of pathological fibrosis in different organs. *In vivo*, mechanical stimuli from the extracellular matrix (ECM) are crucial, together with cell-cell contacts and the pro-fibrotic transforming growth factor (TGF)-β1, in promoting fibroblast differentiation. Here, we explore the impact of hydrogels made by polyacrylamide with different composition on fibroblast behavior. By appropriate modulation of the hydrogel composition (e.g. adjusting the crosslinker content), we produce and fully characterize three kinds of scaffolds with different Young modulus (E). We observe that soft hydrogels ($E < 1$ kPa) induced fibroblast differentiation better than stiffer ones, also in the absence of TGF-β1. This study provides a readily accessible biomaterial platform to promote Myof generation. The easy approach used and the commercial availability of the monomers make these hydrogels suitable to a wide range of biomedical applications combined with high reproducibility and simple preparation protocols.

1. Introduction

Hydrogel-based mechanomimetic materials are widely employed as scaffolds to optimize cell culture *in vitro* with a special focus on mimicking the mechanical properties of natural tissues. Indeed, *in vivo* cells are subjected to several interlinked and cross-talking mechanical tensions generated by cell-cell interactions, by internal cell structures (such as the cytoskeleton) or within the extracellular matrix (ECM) [1]. All these mechanical stimuli represent instructive signals modulating a wide range of cell behaviors including viability, motility, spreading and differentiation via a process called mechanotransduction [2]. Among others, cell fate is markedly influenced by the ECM stiffness [3]. Standard *in vitro* cell cultures are generally performed on glass or plastic supports which are characterized by stiffness values (Young modulus, E, 1–10 GPa) very far from the native ones (mostly in the kPa range) [4]. Therefore, conventional substrates do not account for the tissue ECM mechanics, calling for new mechanomimetic scaffolds. Among them, hydrogels made from either natural or synthetic sources are the most promising [5]. In the former class, collagen, hyaluronic acid or fibrin based hydrogels are studied for replicating both composition and ECM stiffness. However, such materials suffer from a limited range of achievable E values and a lack of independent control among composition and mechanical properties [6]. More importantly, their isolation from natural sources may result in high variability among different batches, leading to a general issue on material reproducibility. Furthermore, the limited stability of these matrices, due to degradation

* Corresponding author.
** Correspondence to: D. Martella, Department of Chemistry "Ugo Schiff", University of Florence, 50019 Sesto Fiorentino, Italy.
E-mail addresses: roberta.squecco@unifi.it (R. Squecco), martella@lens.unifi.it (D. Martella).
[1] These authors contributed equally.

https://doi.org/10.1016/j.bioadv.2023.213674
Received 11 April 2023; Received in revised form 19 October 2023; Accepted 26 October 2023
Available online 29 October 2023

or contraction, can hinder their use in long term cultures [7].

These problems can be overcome by synthetic hydrogels, such as those based on polyethylene glycol or polyacrylamide (PA). These materials allow for a wide range of E values, from tenths to hundreds kPa, thus covering most of the biological tissue stiffness [8]. Mechanomimetic materials are particularly attractive to model the *in vitro* differentiation of myofibroblasts (Myofs) that are recognized as mechanically responsive cells, playing a critical role in the processes of wound healing and fibrosis [9,10]. The latter is a pathological condition that may affect multiple organs with tissue scarring eventually leading to organ function loss [11]. At the moment, a general effective therapy for fibrosis is not present. Despite the heterogeneous fibrotic disease etiology, Myof generation and persistence in an activated state are the recognized core cellular mechanisms of fibrosis in different organs [11]. For this reason, availability of readily accessible in vitro models for Myof generation is crucial for new studies on the tissue repair and fibrosis mechanisms and to develop novel therapeutic treatments. Such models could be also useful in cancer research since these cells are critical elements also in tumor stroma [12].

Myofs are a unique population of cells displaying features of both contractile smooth muscle cells and ECM-synthesizing fibroblasts, hence the name [13]. Among other progenitors, they derive from the differentiation of resident fibroblasts in the ECM [14–17] that is promoted by an integrated action of both mechanical stimuli and different profibrogenic agents, mainly transforming growth factor, TGF-β1. Such compounds are released at the site of a tissue damage by infiltrating inflammatory cells and other local cell types including the same fibroblasts and Myofs [9,18,19]. Notably, also cell-cell communication including gap junction channels have been documented to strongly influence the fibroblasts' transition towards Myofs as well as to be involved in the functional coupling of Myofs to coordinate their activity [20,21].

Fibroblast-to-Myof transition can be reasonably induced *in vitro* by culturing the cells on appropriate scaffolds and supplying TGF-β1 in the culture medium (Fig. 1). Choosing the best scaffolds is challenging since during the physiological tissue repair and fibrosis, ECM undergoes substantial spatio-temporal modifications. Myof generation cannot be assumed as the result of a single mechanical stimulus (from a "final" tissue) but it realistically depends on a more complex process of biological tissue softening (e.g. after injury) and stiffening (e.g. during scar formation). A more detailed overview of the biological Myof generation process is reported in Supplementary Materials (Fig. S1), while Fig. 1 also shows the main biological features that distinguish Myofs from fibroblasts [20,21].

PA scaffolds with different stiffness, ranging from 0.1 to 100 kPa, in combination or not with TGF-β1, have been employed to assess the differentiation of different types of fibroblasts including corneal fibroblasts/keratinocytes [22–24], primary human lung fibroblasts [25–29], portal fibroblasts [30], aortic valvular interstitial cells [31], cardiac fibroblasts [32,33], fibro-adipogenic progenitors [34], mouse embryonic fibroblasts [35–37] and endometrial stromal cells [38]. The majority of these studies showed how stiffer hydrogel (E approximately 10 kPa or more) promotes better Myof differentiation supporting the emerging idea that the ECM stiffening is not only a consequence of fibrosis. In fact, ECM stiffening can itself induce self-reinforcing effects, sustaining Myof differentiation and function and, ultimately, maintaining a pro-fibrotic state. While this explains the progression of an established fibrotic state, it is less clear how the cycle starts [9]. In this scenario, the promotion of Myofs in soft PA hydrogels or other soft matrixes has been also observed [5,33,35,39]. Noteworthy, the number of the studies evaluating PA hydrogels for fibroblast differentiation is still limited, the experimental conditions are very variable (e.g. cell types, gel functionalization, culture media, time of culture) often resulting in a difficult comparison of the results. As well, regarding the scaffold mechanical stiffness, comparison in between different studies is not easy, since they were measured with different techniques (e.g. Atomic Force Microscopy, rheometer) and at different dimensional scales [40]. Finally, most of the current studies are focused on scaffolds mimicking the stiffness of healthy or fibrotic tissues, not considering the natural ECM mechanics soon after wounding or during the wound healing process that fibroblasts experience *in vivo*.

In this article, we aimed to develop an easily reproducible high-throughput *in vitro* model allowing fibroblasts transition to Myofs at best. PA hydrogels with different compositions have been prepared, characterized in terms of mechanical properties and tested as scaffolds for NIH/3T3 fibroblast culture in combination with chemical stimuli, namely TGF-β1. A major finding from our experiments is that hydrogel composition strongly influences differentiation. In particular, hydrogels prepared with low crosslinker amounts promote an efficient differentiation, especially when combined with TGF-β1 and cell-cell communication.

2. Materials and methods

2.1. Hydrogel preparation

All chemical reagents were purchased by Merck and used as received. Three monomer formulations have been prepared by different amounts of acrylamide and *N,N′*-methylenebis(acrylamide) (called later only bis-acrylamide). In 10 mL of water, Stiff hydrogels contain 1.2 g of acrylamide and 25 mg of bis-acrylamide, Medium hydrogels contain 0.8 g of acrylamide and 10 mg of bis-acrylamide and Soft hydrogels contain 500 mg of acrylamide and 2.5 mg of bis-acrylamide. The solutions were degassed and then a 10 % m/V solution of ammonium persulphate (APS) was added to achieve a final concentration of 0.05 % of initiator. At the

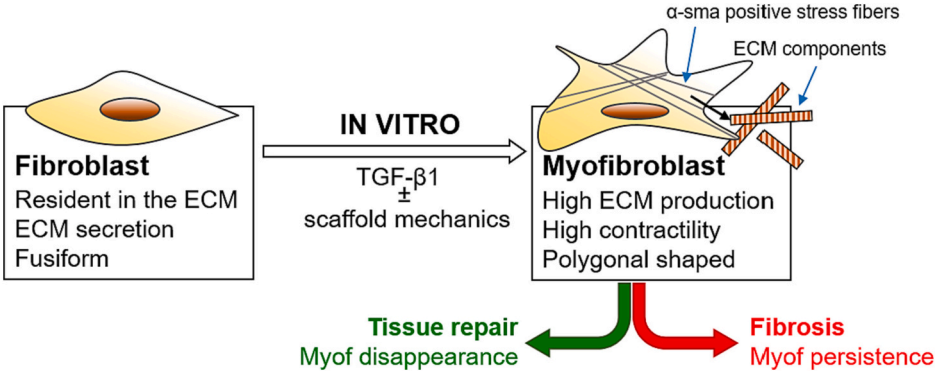

Fig. 1. Scheme of fibroblast-to-Myof differentiation *in vitro*. Myofs display a robust expression of α-smooth muscle actin (α-sma), the actin isoform found in smooth muscle cells, which confers a high contractility to Myofs, incorporated in extensively developed and well-assembled stress fibers. When compared to fibroblasts, differentiated Myofs are larger and secrete higher amounts of ECM components. Moreover, even if Myofs are not regarded as electrically excitable cells, they show distinctive biophysical properties and trans-membrane ion currents typical of smooth muscle cells.

end, a 10 % m/V solution of the *N*,*N*,*N*′,*N*′-tetramethylethylenediamine (TEMED) was added to achieve a final concentration of 0.5 % to induce the polymerization at room temperatures in 20 min. A more detailed procedure to obtain the hydrogel coating on glass coverslip is reported in Supplementary data.

2.2. Hydrogel characterization

Gel fraction indicates the part of the monomeric mixture which is effectively polymerized. It was calculated as the ratio between the weight of the dried gel after immersion in water (to eliminate unpolymerized materials) and the weight of the dried gel before immersion in water according to Eq. (1):

$$Gel\ fraction\ (\%) = \frac{Wf}{Wd} \times 100 \quad (1)$$

where *Wf* is the weight of the hydrogel soaked in water for seven days and then dried at 60 °C for 24 h; *Wd* is the weight of the hydrogel dried at 60 °C for 24 h immediately after the polymerization.

Swelling degree can be described as the water absorptivity of the hydrogel calculated according to Eq. 2:

$$Swelling\ degree\ (\%) = \frac{Ws - Wd}{Ws} \times 100 \quad (2)$$

where *Ws* is the weight of the hydrogel in swollen form; *Wd* is the weight of the hydrogel in dried form.

A scanning electron microscope (SEM, PHENOM-World) was used to observe the hydrogel structures after lyophilization and sputter-coating with a 10 nm gold layer.

2.3. Mechanical test

The mechanical response of fully swollen hydrogels was investigated under shear and compression conditions using a controlled stress rheometer (AR-G2, TA Instruments). All the tests were performed after one-week equilibration of the gels in bi-distilled water [41]. Small amplitude oscillatory shear tests were performed on cylindrical-shaped gel samples. A plate-plate configuration with a Peltier base for temperature control (plate diameter = 25 mm) was adopted. To ensure perfect contact between the sample and the upper tool of the rheometer (no-slip condition), a plate with rough surface was used and the tests were performed under a slight degree of compression. Preliminary analyses were performed to identify a normal force value that did not affect the measurement of the moduli [42]. Preliminary strain sweep tests were carried out to define linear viscoelastic regime, and then the linear viscoelastic shear moduli were recorded at 25 °C in the frequency range $\omega = 5 \times 10^{-2}$–$5 \times 10^{1}$ rad s^{-1}. For uniaxial unconfined compression tests, samples fully submerged in water were squeezed between the parallel plates of the rheometer with a compression rate of 10 μm s^{-1}.

2.4. Cell culture and confocal microscopy analysis

Murine NIH/3T3 fibroblasts, obtained from American Type Culture Collection (ATCC, Manassas, VA, USA), were plated on the different hydrogel substrates and cultured at 37 °C in a humidified atmosphere of 5 % CO_2 for 48 h in media containing different chemical stimuli as follows: in proliferation medium (FBS 10 %) containing Dulbecco's modified Eagle medium (DMEM, Sigma, Milan Italy) enriched with 10 % fetal bovine serum (FBS, Sigma); in low serum condition (FBS 2 %) or in low serum condition in the presence of the pro-fibrotic agent TGF-β1 (2 ng/mL, PeproTech Inc., Rocky Hill, NJ, USA) (differentiation medium, FBS 2 % + TGF-β1). All the media were supplemented with 1 % penicillin/streptomycin (Sigma). Cells grown on glass coverslips were meant as a control. Cells were routinely seeded at a density of 37.5×10^3 cells/cm^2; in some experiments (aimed to avoid cell-cell contact) fibroblasts were seeded at low density (17.5×10^3 cells/cm^2). Confocal laser scanning microscope analyses were performed to reveal F-actin filament organization, α-sma, connexin (Cx)43, collagen type I (Col—I), phosphorylated-small mother against decapentaplegic (pSMAD)-3 expression and cell surface area. Detailed procedures for microscopy observation and cell attachment determination are reported in Supplementary data.

2.5. Electrophysiological records

The records were performed by the whole-cell patch-clamp technique as previously described [21,43]. The resting membrane potential (RMP) was measured in current-clamp mode whereas the passive properties of the cells were assessed in voltage-clamp mode. The passive currents consist of an early capacitive transient due to the membrane capacitance (Cm), followed by a steady-state current flowing through membrane resistance (Rm). The parameter Cm is considered as an index of the cell surface, since the membrane-specific capacitance is supposed to be constant at 1 μF/cm^2. Rm was calculated as already reported [43] and is the parameter related to membrane permeability. Voltage-independent currents flowing through the cell membrane, including ion fluxes through transient receptor potential canonical (TRPC) 1 cationic channels, were evoked by a suitable voltage-clamp step pulse protocol. A more detailed description of electrophysiological techniques used is reported in Supplementary data.

3. Results and discussion

3.1. Scaffold preparation and characterization

The hydrogels were prepared by free radical polymerization starting from a water solution containing acrylamide and bis-acrylamide in different amounts [44,45]. The second component is able to act as a crosslinker between different polymeric chains and it is the main responsible for the mechanical properties of the final material, as shown in Fig. 2a. APS was added as a radical initiator, together with TEMED as co-initiator to trigger the reaction at room temperature. In this condition, the polymerization was completed in 20 min.

During the synthesis, the amount of water and crosslinker were adjusted to obtain three different hydrogels with composition reported in Table 1. The composition is mainly responsible for different mechanical properties of the bulk final materials, that are hereinafter called Stiff, Medium and Soft. The three hydrogels differ for the total monomer concentration and the crosslinking content with both quantities decreasing from the stiffer to the softer materials.

Gel fraction and the equilibrium swelling degree determined by gravimetric methods are reported in Table 1. For the first parameter, we observed a general increase of the gel fraction from 83.5 % to 89.5 % by increasing the monomer concentration in the initial solution. These values indicated that part of the monomers were not bound to the network at the end of the synthesis. The unpolymerized materials can be easily removed by immersion in water. This process has been observed by Attenuated Total Reflectance (ATR) spectroscopy reported, as an example, in Fig. S2. In particular, comparing the spectrum of the monomers with those of the final materials, it is possible to observe the complete disappearance of the band at 816 cm^{-1}, attributed to the -C=C- bending of the polymerizable double bonds. It confirmed the successful removal of unpolymerized monomers during immersion in water. Regarding the swelling degree, the higher amount of crosslinker (passing for the Soft to the Stiff hydrogel) was reflected in a decrease of swelling degree that varies from 96.4 % to 90.1 %.

SEM micrographs in Fig. 2b show the inner microstructure of the gels obtained after freeze-drying. The typical microporous morphology of lyophilized materials is nicely preserved in the Stiff and Medium gels, while partial collapse of the pores can be appreciated for the Soft gel. This difference in the self-supporting ability of the three systems can be

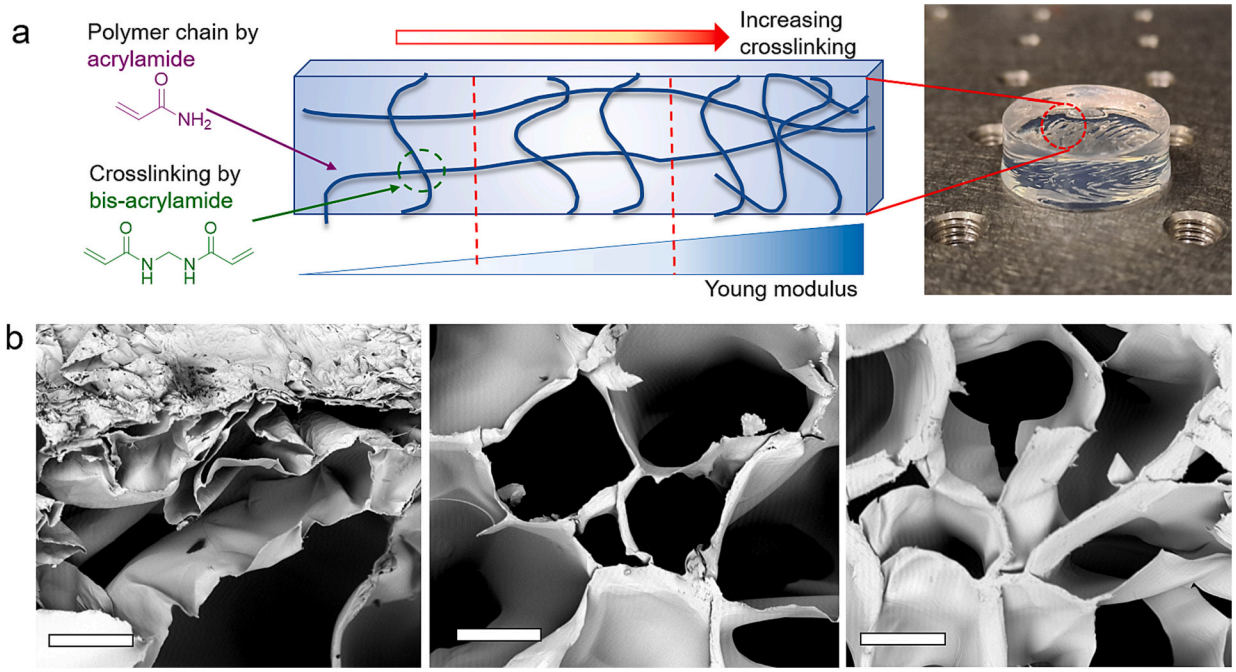

Fig. 2. Composition and structure of the hydrogels. a) Picture of a hydrogel and scheme of the material structures; b) SEM images of hydrogels after drying (Soft, Medium and Stiff hydrogel form left to right), scale bars: 80 μm.

Table 1
Composition and swelling capabilities of hydrogels. [a] % are indicated in weight over the water volume. All samples contain the same amount of APS (0.05 %) and TEMED (0.5 %). [b] Values are expressed as the mean ± standard deviation of three samples.

Hydrogel	Acrylamide (%)[a]	Bis-acrylamide (%)[a]	Gel fraction (%)[b]	Swelling degree (%)[b]
Stiff	12	0.25	89.5 ± 0.4	90.1 ± 0.4
Medium	8	0.1	86.7 ± 0.6	94.1 ± 0.4
Soft	5	0.025	83.5 ± 0.4	96.4 ± 0.4

taken as a first, indirect measure of the different mechanical response of the investigated systems.

More quantitative details on the mechanical behavior were obtained by shear and compression measurement on fully swollen samples. Oscillatory shear tests were performed to measure the linear viscoelastic moduli of the gels. In particular, the elastic (G') and loss (G") shear moduli are shown in Fig. 3a as a function of the oscillatory frequency. All the samples exhibit the typical fingerprint of irreversibly covalently crosslinked gel-like materials: both moduli are essentially frequency-independent, with G' > G" over the entire investigated frequency range, pointing out that the elastic response of the hydrogels is more pronounced than the viscous one. This conclusion is further corroborated by the data in Fig. 3b, in which the phase angle (δ), that represents the lag between the stimulus (stress) and the response (strain) during the oscillatory test, is reported as a function of the oscillatory frequency. Since it is defined as $tan\delta = G''/G'$, the phase angle is a relative measure of the viscous and elastic properties of a material. Its value can span between 0 and 90°, with the two extreme behaviors characterizing the response of a purely elastic and purely viscous material, respectively.

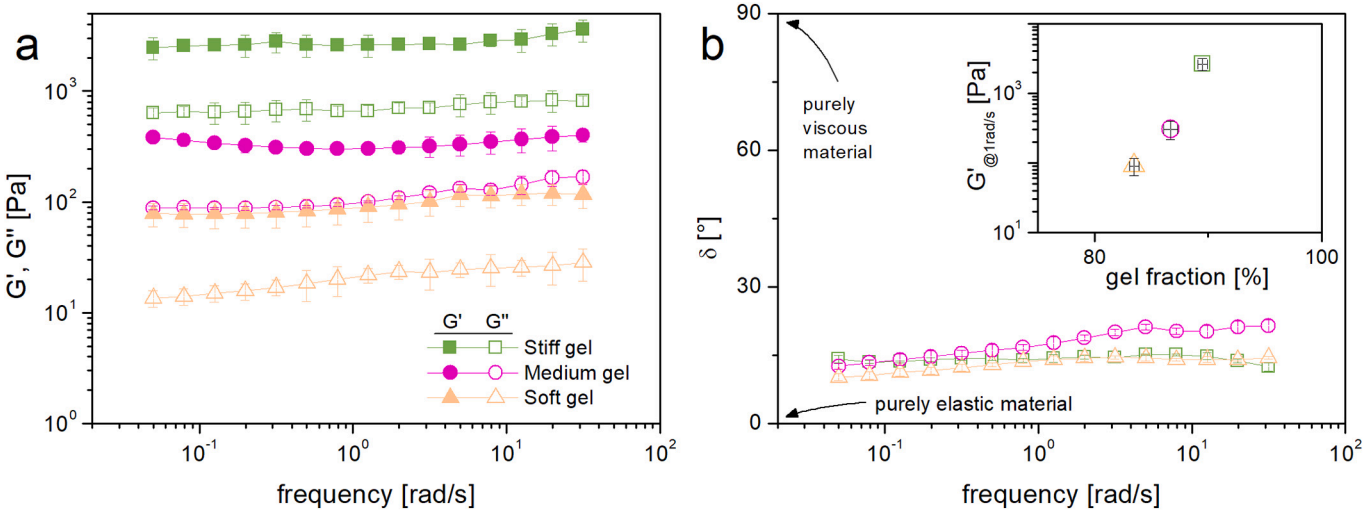

Fig. 3. Small amplitude oscillatory shear tests on hydrogels. Frequency dependence of a) the viscoelastic shear moduli and b) the phase angle for the three gels. The inset in b) shows the elastic shear modulus at 1 rad s^{-1} as a function of the gel fraction.

Besides being all characterized by comparable values of the phase angle, the low value of δ indicates that all the investigated gels can be mainly regarded as elastic materials. Moreover, it is also evident that the increase of the bisacrylamide-to-acrylamide ratio led to a higher cross-linking degree and, hence, higher values of the elastic shear modulus (inset of Fig. 3b).

Hence, viscous or viscoelastic features of the material can be considered negligible at least within the timescales of interest. To rule out poroelastic phenomena, related to the frictional drag that can be generated from the water flows through the polymeric network during tests, compression measurements were performed on submerged samples. In this framework, a neoHookean hyperelastic model can be assumed, as it is typically done for most hydrogel materials [46,47]. Compression tests can be hence exploited to measure the elastic modulus of the gels [45]. Fig. 4 shows the compressive stress-strain curves of the gels, in which true (Cauchy) stress (σ_{true}) and strain (ε_{true}) were calculated from the applied force and uniaxial displacement exploiting the following relationships [48]:

$$\sigma\ true = \frac{F}{A_0[1 - 2v\frac{\Delta h}{h_0}]}.$$

$$\varepsilon\ \text{true} = ln\left(\frac{h}{h_0}\right)$$

in which A_0 and h_0 represent the initial cross section and height of the sample, F and $\Delta h = (h - h_0)$ are the normal force and displacement that were recorded during the compression test, and a Poisson's ratio of $= 0.49$ is assumed in accordance with the previous considerations. From the σ_{true}-ε_{true} curve at compression, the Young's modulus (E_c) can be finally determined from the slope of the curve in the small-deformations range in which samples exhibit linear behavior, and it is reported in the inset of Fig. 4 as a function of gel fraction) [49].

To sum up, the measured mechanical properties of the hydrogels are summarized in Table 2.

The hydrogels have been prepared as thin layers over glass coverslips to enable the biological tests. The schemes of the whole preparation protocol are reported in Figs. S3 and S4. First, the glass coverslips have been treated with (3-methacryloxypropyl)trimethoxysilane (MAPTMS) to enhance the adhesion of the polymeric gels and to avoid its detaching during the cell cultures (Fig. S3) [50]. Later, a drop of the hydrogel formulation solution was placed on a Mylar film and then, a treated glass was gently placed on the top of it. In this way, the drop spread over the whole glass surface and, after waiting the polymerization time, the Mylar was removed leading to the hydrogel coating on the other surface with a thickness higher than 10 μm (Fig. S5).

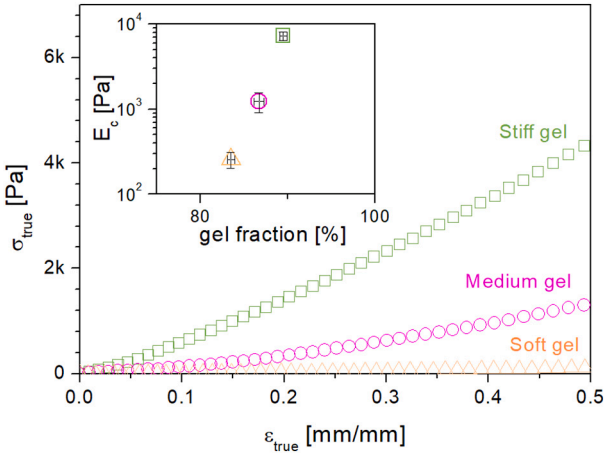

Fig. 4. Unconfined compression tests on hydrogels. Stress-strain compression curves for the three hydrogels. The elastic modulus at compression is reported in the inset as a function of the gel fraction.

Table 2
Summary of the mechanical properties of the investigated hydrogels.

Hydrogel	G' @ 1 rad s^{-1} [kPa]	E_c [kPa]
Stiff	2.61 ± 0.49	7.22 ± 0.85
Medium	0.30 ± 0.09	1.23 ± 0.32
Soft	0.09 ± 0.02	0.26 ± 0.05

3.2. Morpho-functional evaluation of fibroblast to Myof differentiation

The experiments were performed with NIH/3T3 fibroblasts. This immortalized murine cell line is a prevalent model system for studying fibroblast behavior. Previous research by some of us demonstrated that this cell line responds to TGF-β1 stimulation similarly to human dermal and primary cardiac fibroblasts [21,51]. NIH/3T3 fibroblasts were seeded directly on the prepared scaffolds and on glass coverslips (standard support as control). A first test demonstrated the hydrogels to support NIH/3T3 cells attachment with a very similar behavior on all the formulations. In particular, cell attachment percentage (determined as reported in Supplementary data) has been calculated as 74.2 % ± 2.6, 74.3 % ± 2.4 and 75.6 % ± 2.0, for the Stiff, the Medium and Soft hydrogel, respectively. For differentiation test, cells were cultured for 48 h in three different experimental conditions: (i) proliferation medium containing high concentration of fetal bovine serum (FBS 10 %), (ii) low serum medium (FBS 2 %), and (iii) low serum medium containing the pro-fibrotic agent TGF-β1 (differentiation medium, FBS 2 % + TGF-β1). The last condition was demonstrated to induce *in vitro* the transition of fibroblasts towards differentiated Myofs on the conventional culture glass or plastic dishes [20,21]. Usually, in low serum condition the cells reduce their capability to grow and proliferate while starting to differentiate. Notably the low serum condition may likely mimic the microenvironment to whom the cells are subjected after tissue wounding. The use of media of different (serum) compositions, like proliferation and low serum media, allowed us to better discern the effects induced by the substrate itself from those promoted by the chemical profibrotic agents. On the other hand, culturing the cells in differentiation medium containing TGF-β1 allowed us to assess the effects of the combination of scaffold composition and chemical stimuli. The effective transition of NIH/3T3 fibroblasts towards Myofs was assayed by morphological and immunocytochemical analyses (Figs. 5,6 and 7, Fig. S6), and further corroborated by a functional electrophysiological characterization (Fig. 8). Exemplificative confocal images and quantitative analysis of F-actin and α-smooth muscle actin (α-sma, the most reliable marker of well differentiated Myof) are reported in Figs. 5 and 6, respectively. Cell surface area is quantified in Fig. 6q by a morphometric analysis on Differential Interference Contrast (DIC) images (examples are reported in Fig. 6m-o).

Fibroblasts cultured on glass coverslips in FBS 10 % for 48 h showed the typical spindle-like shape, did not exhibit assembled cytoskeletal stress-fiber structures as judged by F-actin staining (Fig. 5a) and expressed very low levels of α-sma. This protein appeared with a punctiform/dot-like staining and mainly dispersed throughout the cytoplasm (Fig. 6a).

When cultured in FBS 2 % cells showed changes in the shape becoming mostly polygonal. They also displayed thin F-actin positive stress fiber-like structures suggesting their activation as proto-Myofs (Fig. 5e). This intermediate type of Myof is usually formed just after a tissue damage, as a consequence of ECM mechanical stress, and later undergoes mature differentiation thanks to the action of TGF-β1. An increase of α-sma expression was also detected (Fig. 6e).

As expected, when cultured in FBS 2 % + TGF-β1 the cells appeared fully differentiated as Myofs. Indeed, they showed a prominent stress fiber network across cytoplasm (Fig. 5i) concomitantly to a robust

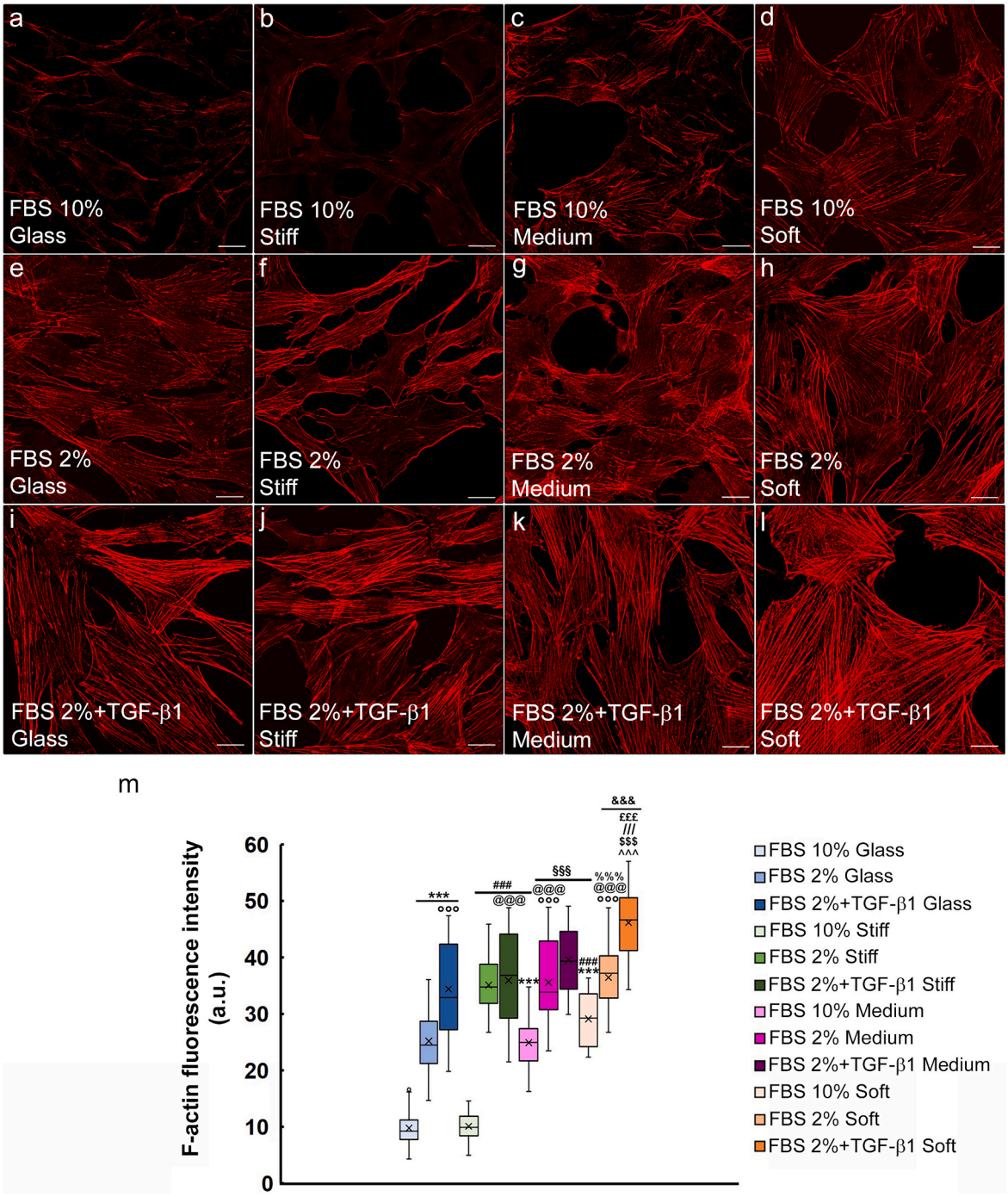

Fig. 5. Morphological analyses of NIH/3T3 fibroblast-to-Myof transition: cytoskeletal F-actin assembly. a-l) Representative confocal immunofluorescence images of fixed cells incubated with TRITC-labeled phalloidin to stain F-actin. Scale bars: 20 μm. m) Densitometric analysis of the fluorescence intensity (in arbitrary units, a.u.) of F-actin. Data are the mean ± SD. One-way ANOVA with Tukey's post hoc test. *** $p < 0.001$ vs FBS 10 % Glass; °°° $p < 0.001$ vs FBS 2 % Glass; $$$ $p < 0.001$ vs FBS 2 % + TGF-β1 Glass; ### $p < 0.001$ vs FBS 10 % Stiff; @@@ $p < 0.001$ vs FBS 2 % Stiff; /// $p < 0.001$ vs FBS 2 % + TGF-β1 Stiff; §§§ $p < 0.001$ vs FBS 10 % Medium; %%% $p < 0.001$ vs FBS 2 % Medium; £££ $p < 0.001$ vs FBS 2 % + TGF-β1 Medium; &&& $p < 0.001$ vs FBS 10 % Soft; ^^^ $p < 0.001$ vs FBS 2 % Soft.

expression of α-sma well organized along stress fibers (Fig. 6i), a more polygonal shape and an increase of the cell surface area. These results on fibroblast behavior have been the starting point of our scaffold exploration to find a material able to further improve the Myof phenotype acquisition. For this reason, the same culture conditions have been repeated using the hydrogels as scaffolds. To note that, hydrogels thinner than 10 μm have not been tested since, in these cases, the underlying glass stiffness may affect the cell differentiation process [52]. As observed on glass support, when fibroblasts were grown on the hydrogels, they became activated and displayed the Myof features after shifting from FBS 10 % to FBS 2 % and especially to FBS 2 % + TGF-β1. In particular, the cells cultured on Stiff hydrogel (Fig. 5b,f,j and Fig. 6b,f,j) behaved quite similar to the cells on Glass, although they expressed low levels of α-sma after culturing in FBS 2 % + TGF-β1 (Fig. 6j).

On Medium hydrogel, the cells showed a more pronounced tendency to become activated and to undergo differentiation, exhibiting an increased F-actin staining and assembling already in FBS 10 % and in FBS 2 %, as compared to Glass in the same culture media (Fig. 5c,g).

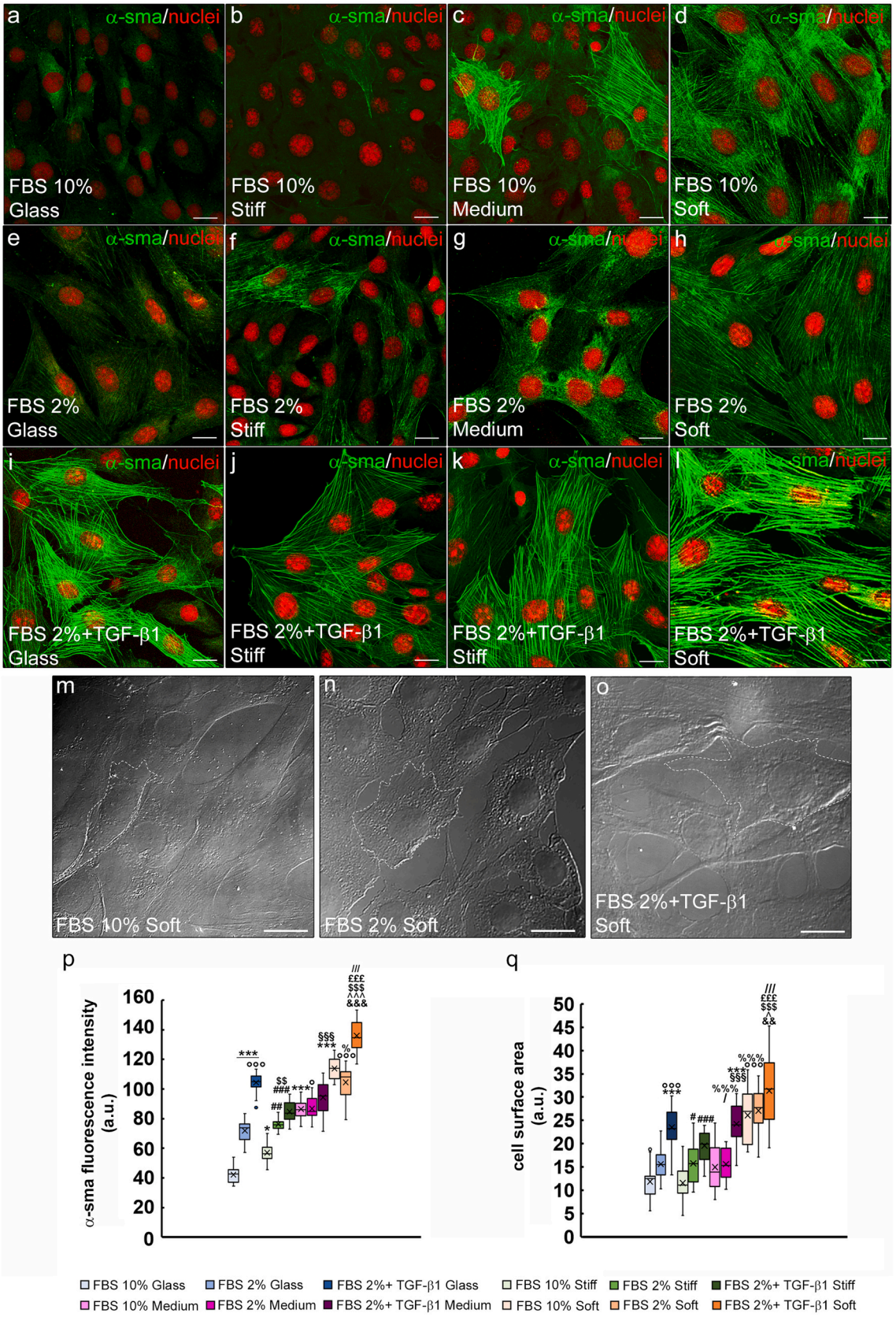

(caption on next page)

Fig. 6. Morphological analyses of NIH/3T3 fibroblast-to-Myof transition: α-sma expression and cell surface area. a-l) Representative confocal immunofluorescence images of fixed cells immunostained with antibodies against α-sma (green). Nuclei are counterstained in red with propidium iodide. Scale bars: 20 μm. m-o) Representative differential interference contrast (DIC, gray) images of fixed cell cultured on Soft hydrogels in the indicated experimental condition and observed under the confocal scanning laser microscopy. White dotted lines were depicted to better visualize the cell shape. Scale bars: 25 μm. p) Densitometric analysis of the fluorescence intensity (in arbitrary units, a.u.) of α-sma. q) Morphometric analysis of mean cell surface area in a.u. Data are the mean ± SD. One-way ANOVA with Tukey's post hoc test. * $p < 0.05$, *** $p < 0.001$ vs FBS 10 % Glass; ° $p < 0.05$, °°° $p < 0.001$ vs FBS 2 % Glass; $$ $p < 0.01$, $$$ $p < 0.001$ vs FBS 2 % + TGF-β1 Glass; # $p < 0.05$, ## $p < 0.01$, ### $p < 0.001$ vs FBS 10 % Stiff; / $p < 0.05$, /// $p < 0.001$ vs FBS 2 % + TGF-β1 Stiff; §§§ $p < 0.001$ vs FBS 10 % Medium; % $p < 0.05$, %% % $p < 0.001$ vs FBS 2 % Medium; £££ $p < 0.001$ vs FBS 2 % + TGF-β1 Medium; && $p < 0.01$, &&& $p < 0.001$ vs FBS 10 %Soft; ^ $p < 0.05$, ^^^ $p < 0.001$ vs FBS 2 % Soft. (For interpretation of the references to color in this figure legend, the reader is referred to the web version of this article.)

Moreover, in FBS 10 %, they exhibited a concomitant increase of α-sma expression as compared to Glass (Fig. 6c). The cell behavior on Medium hydrogel in FBS 2 % + TGF-β1 was comparable to that of the cells cultured with the same medium on Glass (Figs. 5k, 6k).

Finally, when cells were plated on Soft hydrogel, we observed a robust increase of stress fiber formation and organization, as well as of α-sma expression levels and distribution along the filamentous structures. This was noted both in FBS 10 % (Figs. 5d and 6d,m) and in FBS 2 % (Figs. 5h and 6h,n) as compared to Glass, and even compared to Medium hydrogel in the same media.

These findings suggest a key role for hydrogel composition itself, especially of Soft one, in prompting fibroblast activation and the subsequent transition to Myofs, that might likely be elicited by the recruitment and activation of pro-fibrotic mechanotransduction pathways.

Notably, the cells cultured on Soft hydrogel in the presence of TGF-β1 (FBS 2 % + TGF-β1) underwent the optimal differentiation displaying the best typical features of well differentiated Myofs. Indeed, they appeared polygonal, exhibited thick and well aligned parallel F-actin containing stress-fibers (Fig. 5l) with high levels of α-sma and an increased cell surface area as compared to that shown by cells cultured on other substrates in FBS 2 % + TGF-β1 (Fig. 6l,o).

To better characterize Myof phenotype acquired on Soft hydrogel, we evaluated further distinctive markers such as Col-I and Cx43 (Fig. 7). Collagen proteins, in fact, are secreted in higher amounts by differentiated Myofs compared to fibroblasts [18], while Cx43 is a typical Cx forming voltage-dependent connexons, whose expression usually increases in Myof pairs in parallel with gap junction channel functionality [20,21]. The results indicates that the cells on Soft hydrogel showed a robust increase in the expression of Col-I at the cytoplasmic level and, in FBS 2 % + TGF-β1, even outside the cells in a filamentous form as compared to cells cultured on Glass, typical of mature Myofs in an active ECM synthesizing phase (Fig. 7a-f,m). Of note, the cells plated on Soft hydrogels displayed also an increased expression of Cx43 as compared to the cells on Glass. This difference was particularly pronounced when cells were cultured in the absence of TGF-β1 (Fig. 7g-l,n). Cx43 appeared localized both at the cytoplasmic level and at the cell membrane level of adjacent cells, in agreement with previous results [20,21]. In contrast, in the presence of TGF-β1, cells on Soft hydrogel and Glass exhibited a comparable expression of Cx43.

Moreover, we evaluated the behavior of the cells cultured at low density, thus minimizing the impact of cell-cell contacts. Morphological analysis clearly revealed that sparse cells on Soft hydrogel appeared more differentiated as compared to the cells on Glass in the same medium (Fig. S6). Finally, to verify whether the response of the cells to the Soft substrate not stimulated by exogenous TGF-β1 could be dependent to the TGF-β1 possibly contained in the FBS, we analyzed the activation of the canonical TGF-β1/SMAD signaling pathway [53]. We found that the cells cultured on Soft hydrogel in proliferation and low serum medium condition did not show activation of such signaling pathway not exhibiting nuclear expression of the downstream effectors of TGF-β1 namely pSMAD-3, contrary to the cells cultured in the presence of TGF-β1 (Fig. S7) further supporting the impact of the substrate on the promotion of fibroblasts to Myof transition.

Altogether, the morphological observations strongly suggest that fibroblast to Myof transition was mostly due to an integrated and synergistic action between the scaffold composition and chemical stimuli, namely signaling downstream of TGF-β1.

Furthermore, the functional acquisition of the Myof phenotype was assessed by the whole-cell patch- clamp technique (Fig. 8) [51]. Since morphological analyses indicated the Soft hydrogel as the best scaffolde, we here present electrophysiological investigations performed only on contacting cells plated on this substrate and on Glass for comparison. To estimate the appearance of features more typical of excitable cells, as Myofs can be considered, we first evaluated changes in the RMP, index of cell excitability, during the fibroblasts to Myof transition. We observed that cells cultured on Glass in FBS 2 % + TGF-β1 showed a more depolarized RMP compared with those grown in FBS 10 % in accord with previously published data [54], confirming the reliability of the model to differentiate under the classical pro-fibrotic chemical stimulus. Of note, this trend was endorsed also for cells plated on Soft hydrogel scaffolds. Notably, when cells were cultured on this hydrogel, their membrane was more depolarized if compared to those plated on Glass (Fig. 8b). This can indicate that Soft substrate is even more effective in promoting a better Myof differentiation than the standard supports, enabling cells to gain a membrane potential value that is closer to the contractile activation threshold.

Then, we analyzed the Cm that is the passive property usually considered as an index of membrane surface extension being approximately related to cell size and surface morphology. As expected, according to the morphological analysis, cells cultured in FBS 2 % + TGF-β1 showed significantly higher Cm values compared to those grown on FBS 10 %, confirming an increased size for Myofs (Fig. 8d). This tendency was observed for cells plated on both Glass and Soft hydrogel. All these parameter values are listed in Table 3. When we compared cells cultured in the same medium, FBS 2 % + TGF-β1, we found no significant differences between those plated on Glass and those on Soft hydrogel ($p = 0.32$ Glass vs Soft), suggesting that Soft hydrogel seems not to be much more effective than Glass in determining an increase in Cm.

Next, we measured the Rm, that is an index of membrane permeability. We observed that Rm values increased during differentiation (FBS 2 % + TGF-β1) as compared to those cultured in FBS 10 % for both types of supports (Fig. 8e). Although cells grown in FBS 2 % + TGF-β1 on the different substrates did not show statistically significant differences, we observed a higher variability of Rm values on cells grown on glass coverslips. In contrast, Rm values measured from cells on Soft hydrogel (in FBS 10 % and FBS 2 %) were more homogeneous. This may suggest that Soft hydrogel drives a more uniform differentiation of Myofs, usually presenting heterogeneous cell populations.

The occurrence of specific ion currents can be a further index of differentiation [53]. Representative current responses from cells grown on Glass (Fig. 8f) and on Soft hydrogel (Fig. 8g) have been recorded both in FBS 10 % and FBS 2 % + TGF-β1. These linear current time courses put in evidence the non-voltage dependent currents, likely including those flowing through mechanically activated non selective cation channels, such as TRPC1 channels. Our preliminary records show that the overall current size increases during differentiation, especially on the Soft hydrogel. On the bases of the larger current amplitude and the more negative baseline current recorded on Soft hydrogel as compared to Glass, we can deduce a different stimulation of the cell membrane channels, most likely the mechanosensitive ones. This result strongly

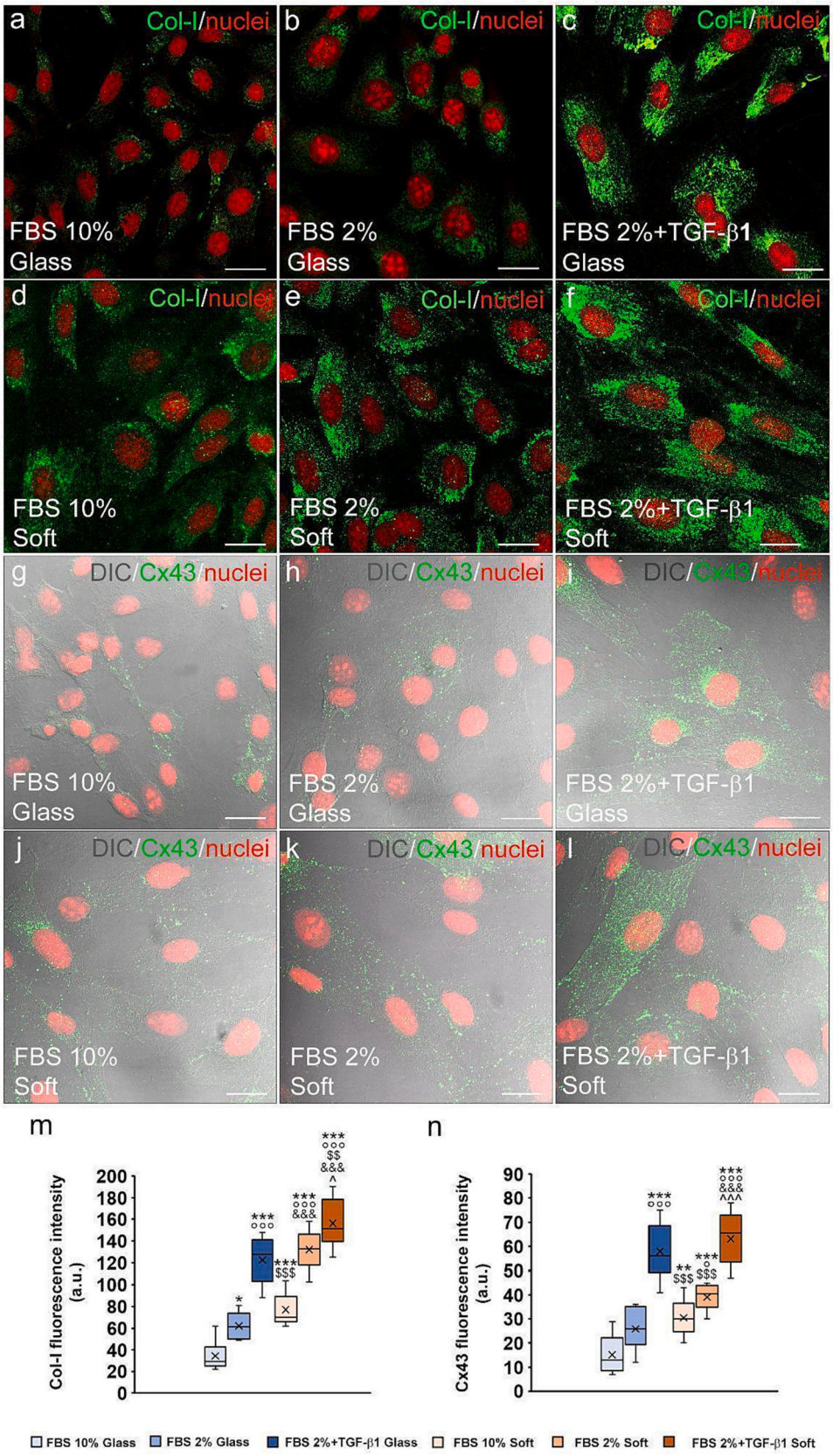

(caption on next page)

Fig. 7. Morphological analyses of NIH/3T3 fibroblast-to-Myof transition: Col-I and CX43 expression. a-f) Representative confocal immunofluorescence images of fixed cells immunostained with antibodies against Col-I (green). Nuclei are counterstained in red with propidium iodide (PI). Scale bars: 25 μm. g-l) Representative superimposed differential interference contrast (DIC, gray) and confocal fluorescence images (acquired simultaneously) of the cells immunostained with antibodies against Cx43 (green) and counterstained with PI to label nuclei. Scale bars: 25 μm. m,n) Densitometric analyses of the fluorescence intensity (in arbitrary units, a.u.) of Col-I and Cx43. Data are the mean ± SD. One-way ANOVA with Tukey's post hoc test. * $p < 0.05$, ** $p < 0.01$, *** $p < 0.001$ vs FBS 10 % Glass; ° $p < 0.05$, °°° $p < 0.001$ vs FBS 2 % Glass; $$$ $p < 0.001$ vs FBS 2 % + TGF-β1 Glass; &&& $p < 0.001$ vs FBS 10 % Soft; ^ $p < 0.05$, ^^^ $p < 0.001$ vs FBS 2 % Soft. (For interpretation of the references to color in this figure legend, the reader is referred to the web version of this article.)

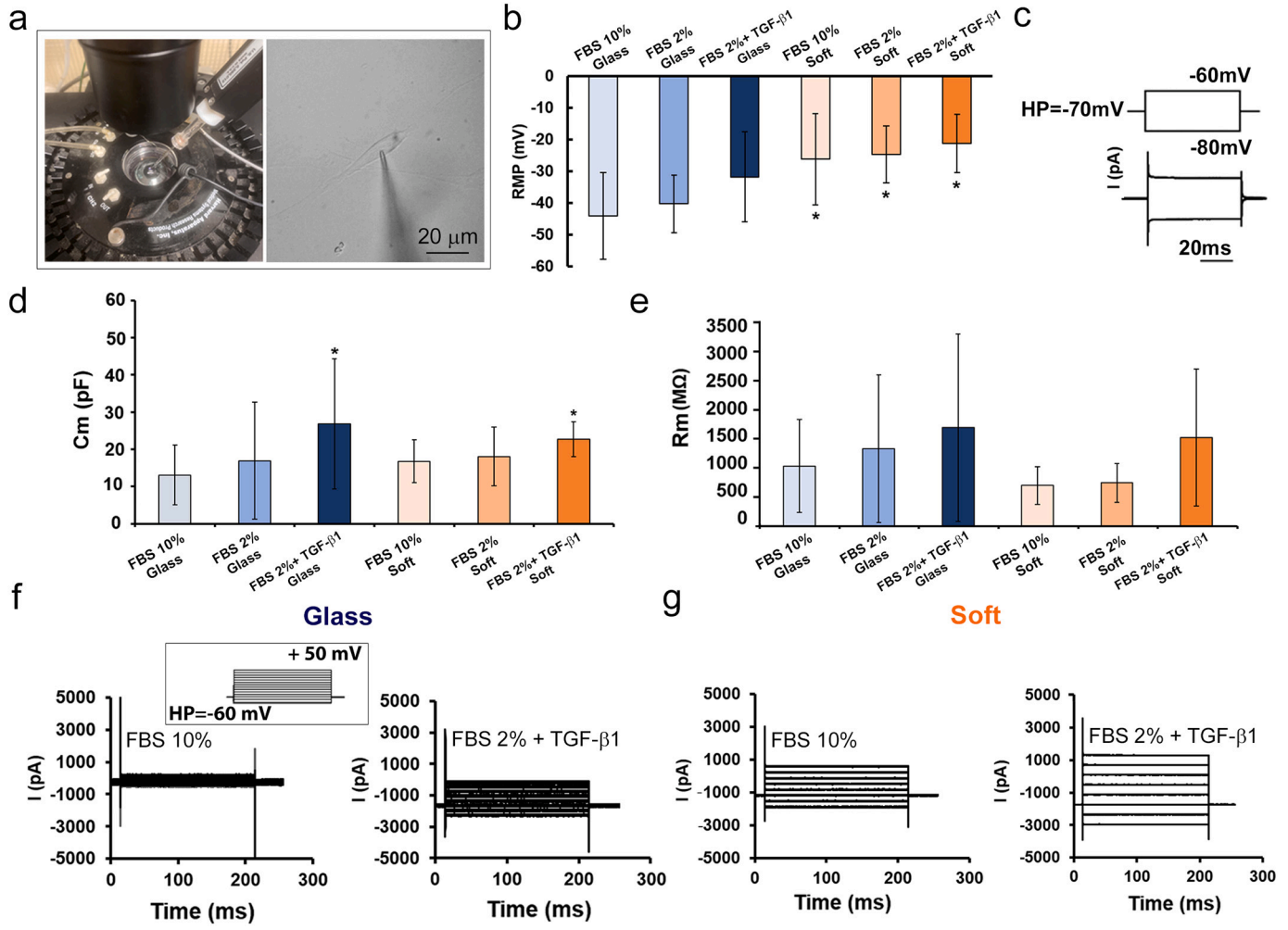

Fig. 8. Electrophysiological records. a) Left panel: Detail of the experimental chamber with cells plated on the coverslip and patch pipette approaching the cell surface. Right panel: light microscopy image of a representative patched fibroblast (Scale bar: 20 μm). b) RMP (in mV), evaluated in current clamp condition (current stimulus $I = 0$ nA) from cells plated on different substrates (Glass, left bar charts in blue scale color; Soft hydrogels, right bar charts in orange scale color) and cultured in different media - proliferation medium (FBS 10 %), low serum medium (FBS 2 %) and differentiation medium (FBS 2 % + TGF-β1). c) Voltage pulse protocol of stimulation (top) and representative passive current responses (bottom). d) Cm, values (in pF) and e) Rm, values (in MΩ), obtained from cells plated on different substrates (Glass, left bar charts in blue scale color; Soft hydrogels, right bar charts in orange scale color) and cultured in the different media. Data are mean ± SD. Two- way ANOVA with Bonferroni 's correction. *$p < 0.05$ vs FBS 10 % Glass. f) Representative time courses of currents (in pA) recorded from a cell grown on Glass coverslips in FBS 10 % (left) and in FBS 2 % + TGF-β1 (right). Pulse protocol of stimulation shown in the inset. These current responses include ionic fluxes through TRPC channels. g) Representative time courses of currents (in pA) recorded from a cell grown on Soft hydrogel in FBS 10 % (left) and FBS 2 % + TGF-β1 (right). (For interpretation of the references to color in this figure legend, the reader is referred to the web version of this article.)

suggests that different supports provoke a dissimilar stimulation of the mechanically-activated channels that may differently contribute to the interplay guiding differentiation.

4. Conclusions

To sum up, we here intend to present a readily accessible biomaterial platform to promote fibroblast to Myof differentiation. Accordingly, we prepared and characterized three different polyacrylamide hydrogels with elastic modulus at compression in between 0.26 and 7.22 kPa. The materials have been tested as scaffolds for NIH/3T3 fibroblast culture (48 h) showing that, also in the absence of the pro-fibrotic agent TGF-β1, a better differentiation towards Myofs can be achieved on softer substrates. Indeed, this kind of hydrogel was able to activate by itself F-actin positive stress fiber formation, to induce α-sma expression and organization in filamentous structures and to increase Col-I synthesis and Cx43 expression. The acquisition of a more differentiated phenotype was supported also by the functional electrophysiological analyses revealing that cells cultured on Soft hydrogel acquired Myof plasmamembrane features better than those seeded on Glass support.

Table 3
Effects of the different treatments and substrates on passive properties of NIH/3 T3 cells. Data are as mean ± SD. *$p < 0.05$ vs. FBS 10 % Glass, (Two-way ANOVA with Bonferroni's correction). n = number of cells.

	FBS 10 % Glass	FBS 2 % Glass	FBS 2 % + TGF-β1 Glass	FBS 10 % Soft	FBS 2 % Soft	FBS 2 % + TGF-β1 Soft
RMP (mV)	−44.1 ± 13.6 (n = 9)	−40.4 ± 8.9 (n = 8)	−31.9 ± 14.2 (n = 20)	−26.3 ± 14.4* (n = 18)	−24.8 ± 8.9* (n = 10)	−21.3 ± 9.2* (n = 12)
Cm (pF)	13.1 ± 7.9 (n = 10)	16.9 ± 15.7 (n = 8)	26.8 ± 17.4* (n = 22)	16.8 ± 5.8 (n = 15)	18.1 ± 7.9 (n = 8)	22.7 ± 4.7* (n = 7)
Rm (MΩ)	1034.4 ± 800.0 (n = 11)	1331.0 ± 1267.4 (n = 4)	1692.3 ± 1612.9 (n = 20)	697.4 ± 326.4 (n = 15)	744.3 ± 330.2 (n = 8)	1519.4 ± 1176.6 (n = 11)

However, a limitation of the present *in vitro* model is the lack of precise control over the adhesive cues presented by the hydrogels. The control of the type and density of adhesive ligands present on the surface would allow us to discern deeply both the involvement of adhesive ligand-cell receptor interactions and the role of the scaffold stiffness in driving the differentiation. Nevertheless, we can currently speculate that the changes we observed in the cell behavior on the different substrates may be correlated to the stiffness differences. Soft hydrogel may resemble the mechanical properties occurring as soon after a tissue lesion (namely ECM destruction or disorganization and reduced ECM stiffness) that represents the first stimulus for activating the cells into a repairing myofibroblastic phenotype. Support on this hypothesis would be given by the functionalization of the hydrogels with adhesive cues such as collagen or fibronectin. Experiments are ongoing in our lab to assess the effects of different coatings. Indeed, it should be kept in mind that different adhesive molecules may interfere with the cell response [55], eliciting dissimilar outcomes likely by activating different downstream mechanotransduction signaling. Furthermore, adhesive coatings may certainly improve cell adhesion which could be very helpful when using other cell types (e.g. primary ones) and for longer term cell culture.

Abbreviations

APS	ammonium persulphate
α-sma	smooth muscle actin
ATCC	American Type Culture Collection
ATR	Attenuated Total Reflectance
Cm	Cell capacitance
Col-I	Collagen type-I
Cx43	Connexin 43
DIC	Differential Interference Contrast
DMEM	Dulbecco's modified Eagle medium
E	Young Modulus
ECM	Extracellular matrix
FBS	Fetal bovine serum
HP	Holding potential
MAPTMS	3-(Trimethoxysilyl)propyl methacrylate
Myof	Myofibroblast
PA	Polyacrylamide
pSMAD	phosphorylated small mother against decapentaplegic
Rm	Membrane resistance
RMP	Resting membrane potential
TEMED	*N,N,N′,N′*-tetramethylethylenediamine
SEM	Scanning electron microscopy
TGF	Transforming growth factor
TRPC	Transient receptor potential canonical
ν	Poisson's coefficient.

CRediT authorship contribution statement

Alice Cappitti: Investigation, Methodology. **Francesco Palmieri:** Formal analysis, Investigation, Methodology, Writing – original draft. **Rachele Garella:** Investigation, Methodology. **Alessia Tani:** Investigation, Methodology. **Flaminia Chellini:** Data curation, Formal analysis, Funding acquisition, Writing – original draft. **Martina Salzano De Luna:** Investigation, Data curation, Writing – original draft. **Camilla Parmeggiani:** Funding acquisition, Writing – review & editing. **Roberta Squecco:** Conceptualization, Funding acquisition, Resources, Supervision, Writing – original draft, Writing – review & editing. **Daniele Martella:** Conceptualization, Supervision, Writing – original draft, Writing – review & editing. **Chiara Sassoli:** Conceptualization, Funding acquisition, Resources, Supervision, Writing – original draft, Writing – review & editing.

Declaration of competing interest

The authors declare no competing interest.

Data availability

Data will be made available on request.

Acknowledgment

This work has received funding from Fondazione Cassa di Risparmio di Firenze projects Parmeggiani_2020.1583. The authors acknowledge MIUR-Italy ("Progetto Dipartimenti di Eccellenza 2018−2022" for the funds allocated to the Department of Chemistry "Ugo Schiff" and to the Department of Experimental and Clinical Medicine). This research was also funded by the University of Florence (Fondi di Ateneo-ex 60 %) to Flaminia Chellini, Camilla Parmeggiani, Chiara Sassoli and Roberta Squecco. The authors acknowledge Dr. Sara Nocentini for the profilometer tests.

Appendix A. Supplementary data

Supplementary data contain ATR spectra of the hydrogels, schemes for the scaffold preparation, further details on the experimental procedures, fibroblast-to-Myof differentiation *in vivo* and morphological analysis of cells. Supplementary data to this article can be found online at https://doi.org/10.1016/j.bioadv.2023.213674.

References

[1] S. Weng, J. Fu, Synergistic regulation of cell function by matrix rigidity and adhesive pattern, Biomaterials 32 (2011) 9584–9593, https://doi.org/10.1016/j.biomaterials.2011.09.006.
[2] D.E. Discher, D.J. Mooney, P.W. Zandstra, Growth factors, matrices, and forces combine and control stem cells, Science 324 (2009) 1673–1677, https://doi.org/10.1126/science.1171643.
[3] D.E. Discher, P. Janmey, Y.L. Wang, Tissue cells feel and respond to the stiffness of their substrate, Science 310 (2005) 1139–1143, https://doi.org/10.1126/science.1116995.
[4] W.L. Chen, C.A. Simmons, Lessons from (patho)physiological tissue stiffness and their implications for drug screening, drug delivery and regenerative medicine, Adv. Drug Deliv. Rev. 63 (2011) 269–276, https://doi.org/10.1016/j.addr.2011.01.004.

[5] M.D. Davidson, J.A. Burdick, R.G. Wells, Engineered biomaterial platforms to study fibrosis, Adv. Healthc. Mater. 9 (2020), e1901682, https://doi.org/10.1002/adhm.201901682.

[6] M.E. Smithmyer, L.A. Sawicki, A.M. Kloxin, Hydrogel scaffolds as in vitro models to study fibroblast activation in wound healing and disease, Biomater. Sci. 2 (2014) 634–650, https://doi.org/10.1039/C3BM60319A.

[7] S. Nakagawa, P. Pawelek, F. Grinnell, Long-term culture of fibroblasts in contracted collagen gels: effects on cell growth and biosynthetic activity, J. Invest. Dermatol. 93 (1989) 792–798, https://doi.org/10.1111/1523-1747.ep12284425.

[8] X. Lin, Y. Shi, Y. Cao, W. Liu, Recent progress in stem cell differentiation directed by material and mechanical cues, Biomed. Mater. 11 (2016), 014109, https://doi.org/10.1088/1748-6041/11/1/014109.

[9] L. Van De Water, S. Varney, J.J. Tomasek, Mechanoregulation of the Myofibroblast in wound contraction, scarring, and fibrosis: opportunities for new therapeutic intervention, Adv. Wound Care (New Rochelle). 2 (2013) 122–141, https://doi.org/10.1089/wound.2012.0393.

[10] J.J. Tomasek, G. Gabbiani, B. Hinz, C. Chaponnier, R.A. Brown, Myofibroblasts and mechano-regulation of connective tissue remodelling, Nat. Rev. Mol. Cell Biol. 3 (2002) 349–363, https://doi.org/10.1038/nrm809.

[11] M. Zeisberg, R. Kalluri, Cellular mechanisms of tissue fibrosis. 1. Common and organ-specific mechanisms associated with tissue fibrosis, Am. J. Phys. Cell Phys. 304 (2013) C216–C225, https://doi.org/10.1152/ajpcell.00328.2012.

[12] M. Otranto, V. Sarrazy, F. Bonté, B. Hinz, G. Gabbiani, A. Desmoulière, The role of the myofibroblast in tumor stroma remodeling, Cell Adhes. Migr. 6 (2012) 203–219, https://doi.org/10.4161/cam.20377.

[13] P. Pakshir, N. Noskovicova, M. Lodyga, D.O. Son, R. Schuster, A. Goodwin, H. Karvonen, B. Hinz, The myofibroblast at a glance, J. Cell Sci. 133 (2020) jcs227900, https://doi.org/10.1242/jcs.227900.

[14] V.S. LeBleu, G. Taduri, J. O'Connell, Y. Teng, V.G. Cooke, C. Woda, H. Sugimoto, R. Kalluri, Origin and function of myofibroblasts in kidney fibrosis, Nat. Med. 19 (2013) 1047–1053, https://doi.org/10.1038/nm.3218.

[15] S. Piera-Velazquez, S.A. Jimenez, Endothelial to mesenchymal transition: role in physiology and in the pathogenesis of human diseases, Physiol. Rev. 99 (2019) 1281–1324, https://doi.org/10.1152/physrev.00021.2018.

[16] R.T. Hannan, A.E. Miller, R.C. Hung, C. Sano, S.M. Peirce, T.H. Barker, Extracellular matrix remodeling associated with bleomycin-induced lung injury supports pericyte-to-myofibroblast transition, Matrix Biol. Plus 10 (2020), 100056, https://doi.org/10.1016/j.mbplus.2020.100056.

[17] Y. Tai, E.L. Woods, J. Dally, D. Kong, R. Steadman, R. Moseley, A.C. Midgley, Myofibroblasts: function, formation, and scope of molecular therapies for skin fibrosis, Biomolecules 11 (2021) 1095, https://doi.org/10.3390/biom11081095.

[18] P. Pakshir, B. Hinz, The big five in fibrosis: macrophages, myofibroblasts, matrix, mechanics, and miscommunication, Matrix Biol. 68 (2018) 81–93, https://doi.org/10.1016/j.matbio.2018.01.019.

[19] S.A. Eming, T.A. Wynn, P. Martin, Inflammation and metabolism in tissue repair and regeneration, Science 356 (2017) 1026–1030, https://doi.org/10.1126/science.aam7928.

[20] R. Squecco, F. Chellini, E. Idrizaj, A. Tani, R. Garella, S. Pancani, P. Pavan, F. Bambi, S. Zecchi-Orlandini, C. Sassoli, Platelet-rich plasma modulates gap junction functionality and Connexin 43 and 26 expression during TGF-β1-induced fibroblast to myofibroblast transition: clues for counteracting fibrosis, Cells 9 (2020) 1199, https://doi.org/10.3390/cells9051199.

[21] C. Sassoli, R. Garella, F. Chellini, A. Tani, P. Pavan, F. Bambi, S. Zecchi-Orlandini, R. Squecco, Platelet-rich plasma affects gap junctional features in myofibroblasts in vitro via vascular endothelial growth factor (VEGF)-A/VEGF receptor, Exp. Physiol. 107 (2022) 106–121, https://doi.org/10.1113/EP090052.

[22] B. Dreier, S.M. Thomasy, R. Mendonsa, V.K. Raghunathan, P. Russell, C.J. Murphy, Substratum compliance modulates corneal fibroblast to myofibroblast transformation, Invest. Ophthalmol. Vis. Sci. 54 (2013) 5901–5907, https://doi.org/10.1167/iovs.12-11575.

[23] D.P. Maruri, M. Miron-Mendoza, P.B. Kivanany, J.M. Hack, D.W. Schmidtke, W. M. Petroll, V.D. Varner, ECM stiffness controls the activation and contractility of corneal keratocytes in response to TGF-β1, Biophys. J. 119 (2020) 1865–1877, https://doi.org/10.1016/j.bpj.2020.08.040.

[24] D.P. Maruri, K.S. Iyer, D.W. Schmidtke, W.M. Petroll, V.D. Varner, Signaling downstream of focal adhesions regulates stiffness-dependent differences in the TGF-β1-mediated myofibroblast differentiation of corneal keratocytes, Front. Cell Dev. Biol. 10 (2022), 886759, https://doi.org/10.3389/fcell.2022.886759.

[25] F. Liu, J.D. Mih, B.S. Shea, A.T. Kho, A.S. Sharif, A.M. Tager, D.J. Tschumperlin, Feedback amplification of fibrosis through matrix stiffening and COX-2 suppression, J. Cell Biol. 190 (2010) 693–706, https://doi.org/10.1083/jcb.201004082.

[26] X. Huang, N. Yang, V.F. Fiore, T.H. Barker, Y. Sun, S.W. Morris, Q. Ding, V. J. Thannickal, Y. Zhou, Matrix stiffness-induced myofibroblast differentiation is mediated by intrinsic mechanotransduction, Am. J. Respir. Cell Mol. Biol. 47 (2012) 340–348, https://doi.org/10.1165/rcmb.2012-0050OC.

[27] S. Asano, S. Ito, K. Takahashi, K. Furuya, M. Kondo, M. Sokabe, Y. Hasegawa, Matrix stiffness regulates migration of human lung fibroblasts, Phys. Rep. 5 (2017), e13281, https://doi.org/10.14814/phy2.13281.

[28] K. Wang, L. Shi, W. Linthicum, K. Man, X. He, Q. Wen, L.W. Rojanasakul, Y. Rojanasakul, Y. Yang, Substrate stiffness-dependent carbon nanotube-induced lung fibrogenesis, Nano Lett. 19 (2019) 5443–5451, https://doi.org/10.1021/acs.nanolett.9b01943.

[29] A. Giménez, P. Duch, M. Puig, M. Gabasa, A. Xaubet, J. Alcaraz, Dysregulated collagen homeostasis by matrix stiffening and TGF-β1 in fibroblasts from idiopathic pulmonary fibrosis patients: role of FAK/Akt, Int. J. Mol. Sci. 18 (2017) 2431, https://doi.org/10.3390/ijms18112431.

[30] Z. Li, J.A. Dranoff, E.P. Chan, M. Uemura, J. Sévigny, R.G. Wells, Transforming growth factor-beta and substrate stiffness regulate portal fibroblast activation in culture, Hepatology 46 (2007) 1246–1256, https://doi.org/10.1002/hep.21792.

[31] A.M. Quinlan, K.L. Billiar, Investigating the role of substrate stiffness in the persistence of valvular interstitial cell activation, J. Biomed. Mater. Res. A 100 (2012) 2474–2482, https://doi.org/10.1002/jbm.a.34162.

[32] G. Gilles, A.D. McCulloch, C.H. Brakebusch, K.M. Herum, Maintaining resting cardiac fibroblasts in vitro by disrupting mechanotransduction, PLoS One 15 (2020), e0241390, https://doi.org/10.1371/journal.pone.0241390.

[33] M. Gałdyszyńska, R. Zwoliński, L. Piera, J. Szymański, R. Jaszewski, J. Drobnik, Stiff substrates inhibit collagen accumulation via integrin α2β1, FAK and Src kinases in human atrial fibroblast and myofibroblast cultures derived from patients with aortal stenosis, Biomed. Pharmacother. 159 (2023), 114289, https://doi.org/10.1016/j.biopha.2023.114289.

[34] T. Loomis, L.Y. Hu, R.P. Wohlgemuth, R.R. Chellakudam, P.D. Muralidharan, L. R. Smith, Matrix stiffness and architecture drive fibro-adipogenic progenitors' activation into myofibroblasts, Sci. Rep. 12 (2022) 13582, https://doi.org/10.1038/s41598-022-17852-2.

[35] Y. Li, C.B. Tang, K.A. Kilian, Matrix mechanics influence fibroblast-myofibroblast transition by directing the localization of histone deacetylase 4, Cell. Mol. Bioeng. 10 (2017) 405–415, https://doi.org/10.1007/s12195-017-0493-8.

[36] Y. Yang, K. Xie, H. Jiang, Durotaxis index of 3T3 fibroblast cells scales with stiff-to-soft membrane tension polarity, Biophys. J. 119 (7) (2020) 1427–1438, https://doi.org/10.1016/j.bpj.2020.07.039.

[37] T. Yeung, P.C. Georges, L.A. Flanagan, B. Marg, M. Ortiz, M. Funaki, N. Zahir, W. Ming, V. Weaver, P.A. Janmey, Effects of substrate stiffness on cell morphology, cytoskeletal structure, and adhesion, Cell Motil. Cytoskeleton 60 (1) (2005) 24–34, https://doi.org/10.1002/cm.20041.

[38] S. Matsuzaki, M. Canis, J.L. Pouly, C. Darcha, Soft matrices inhibit cell proliferation and inactivate the fibrotic phenotype of deep endometriotic stromal cells in vitro, Hum. Reprod. 31 (2016) 541–553, https://doi.org/10.1093/humrep/dev333.

[39] C.D. Davidson, D.K.L. Jayco, D.L. Matera, S.J. DePalma, H.L. Hiraki, W.Y. Wang, B. M. Baker, Myofibroblast activation in synthetic fibrous matrices composed of dextran vinyl sulfone, Acta Biomater. 105 (2020) 78–86, https://doi.org/10.1016/j.actbio.2020.01.009.

[40] N.R. Richbourg, M.K. Rausch, N.A. Peppas, Cross-evaluation of stiffness measurement methods for hydrogels, Polymer 258 (2022), 125316, https://doi.org/10.1016/j.polymer.2022.125316.

[41] C. Hernandez, N. Gawlik, M. Goss, H. Zhou, S. Jeganathan, D. Gilbert, A.A. Exner, Macroporous acrylamide phantoms improve prediction of in vivo performance of in situ forming implants, J. Control. Release 243 (2016) 225–231, https://doi.org/10.1016/j.jconrel.2016.10.009.

[42] J.L. Vanderhooft, M. Alcoutlabi, J.J. Magda, G.D. Prestwich, Rheological properties of cross-linked hyaluronan-gelatin hydrogels for tissue engineering, Macromol. Biosci. 9 (2009) 20–28, https://doi.org/10.1002/mabi.200800141.

[43] D. Martella, M. Mannelli, R. Squecco, R. Garella, E. Idrizaj, D. Antonioli, M. Laus, D.S. Wiersma, T. Gamberi, P. Paoli, C. Parmeggiani, T. Fiaschi, Cell instructive liquid crystalline networks for myotube formation, iScience 24 (2021), 103077, https://doi.org/10.1016/j.isci.2021.103077.

[44] R.J. Pelham, Y. Wang, Cell locomotion and focal adhesions are regulated by substrate flexibility, Proc. Natl. Acad. Sci. U. S. A. 94 (1997) 13661–13665, https://doi.org/10.1073/pnas.94.25.13661.

[45] J.R. Tse, A.J. Engler, Preparation of hydrogel substrates with tunable mechanical properties, Curr. Protoc. Cell. Biol. (2010), https://doi.org/10.1002/0471143030.cb1016s47. Chapter 10:Unit 10.16.

[46] K. Upadhyay, G. Subhash, D. Spearot, Thermodynamics-based stability criteria for constitutive equations of isotropic hyperelastic solids, J. Mech. Phys. Solids 124 (2019), https://doi.org/10.1016/j.jmps.2018.09.038, 115-14.

[47] A. Gandin, Y. Murugesan, V. Torresan, L. Ulliana, A. Citron, P. Contessotto, G. Brusatin, Simple yet effective methods to probe hydrogel stiffness for mechanobiology, Sci. Rep. 11 (2021) 22668, https://doi.org/10.1038/s41598-021-01036-5.

[48] C.M. Buffinton, K.J. Tong, R.A. Blaho, E.M. Buffinton, D.M. Ebenstein, Comparison of mechanical testing methods for biomaterials: pipette aspiration, nanoindentation, and macroscale testing, J. Mech. Behav. Biomed. Mater. 51 (2015) 367–379, https://doi.org/10.1016/j.jmbbm.2015.07.022.

[49] D. Lee, H. Zhang, S. Ryu, Elastic modulus measurement of hydrogels, in: M. Mondal (Ed.), Cellulose-based Superabsorbent Hydrogels. Polymers and Polymeric Composites: A Reference Series, Springer, Cham, 2018, https://doi.org/10.1007/978-3-319-76573-0_60-1.

[50] J.M. Pioner, L. Santini, C. Palandri, D. Martella, F. Lupi, M. Langione, S. Querceto, B. Grandinetti, V. Balducci, P. Benzoni, S. Landi, A. Barbuti, F. Ferrarese Lupi, L. Boarino, L. Sartiani, C. Tesi, D.L. Mack, M. Regnier, E. Cerbai, C. Parmeggiani, C. Poggesi, C. Ferrantini, R. Coppini, Optical investigation of action potential and calcium handling maturation of hiPSC-cardiomyocytes on biomimetic substrates, Int. J. Mol. Sci. 20 (2019) 3799, https://doi.org/10.3390/ijms20153799.

[51] R. Squecco, C. Sassoli, R. Garella, F. Chellini, E. Idrizaj, S. Nistri, L. Formigli, D. Bani, F. Francini, Inhibitory effects of relaxin on cardiac fibroblast-to-myofibroblast transition: an electrophysiological study, Exp. Physiol. 100 (2015) 652–666, https://doi.org/10.1113/EP085178.

[52] A. Buxboim, K. Rajagopal, B. Andre, D.E. Discher, How deeply cells feel: methods for thin gels, J. Phys. Condens. Matter 22 (2010), 194116, https://doi.org/10.1088/0953-8984/22/19/194116.

[53] A. Biernacka, M. Dobaczewski, N.G. Frangogiannis, TGF-β signaling in fibrosis, Growth Factors 29 (2011) 196–202, https://doi.org/10.3109/08977194.2011.595714.
[54] C. Sassoli, F. Chellini, R. Squecco, A. Tani, E. Idrizaj, D. Nosi, M. Giannelli, S. Zecchi-Orlandini, Low intensity 635 nm diode laser irradiation inhibits fibroblast-myofibroblast transition reducing TRPC1 channel expression/activity: new perspectives for tissue fibrosis treatment, Lasers Surg. Med. 48 (2016) 318–332, https://doi.org/10.1002/lsm.22441.
[55] V.J. Thannickal, D.Y. Lee, E.S. White, Z. Cui, J.M. Larios, R. Chacon, J.C. Horowitz, R.M. Day, P.E. Thomas, Myofibroblast differentiation by transforming growth factor-beta1 is dependent on cell adhesion and integrin signaling via focal adhesion kinase, J. Biol. Chem. 278 (2003) 12384–12389, https://doi.org/10.1074/jbc.M208544200.